European Journal of Pharmaceutics and Biopharmaceutics 138 (2019) 111–124

Contents lists available at ScienceDirect

European Journal of Pharmaceutics and Biopharmaceutics

journal homepage: www.elsevier.com/locate/ejpb

Research paper

Using microfluidic platforms to develop CNS-targeted polymeric nanoparticles for HIV therapy

Cláudia Martins[a,b,c], Francisca Araújo[a,b,d], Maria João Gomes[a,b,d], Carlos Fernandes[e], Rute Nunes[a,b,d], Wei Li[f], Hélder A. Santos[f,g], Fernanda Borges[e], Bruno Sarmento[a,b,h,*]

[a] i3S – Instituto de Investigação e Inovação em Saúde, Universidade do Porto, Rua Alfredo Allen 208, 4200-135 Porto, Portugal
[b] INEB – Instituto de Engenharia Biomédica, Universidade do Porto, Rua Alfredo Allen 208, 4200-135 Porto, Portugal
[c] FEUP – Faculdade de Engenharia da Universidade do Porto, Rua Dr. Roberto Frias s/n, 4200-465 Porto, Portugal
[d] ICBAS – Instituto Ciências Biomédicas Abel Salazar, Universidade do Porto, Rua de Jorge Viterbo Ferreira 228, 4050-313 Porto, Portugal
[e] CIQUP – Centro de Investigação em Química, Departamento de Química e Bioquímica, Faculdade de Ciências, Universidade do Porto, 4169-007 Porto, Portugal
[f] Drug Research Program, Division of Pharmaceutical Chemistry and Technology, Faculty of Pharmacy, University of Helsinki, Viikinkaari 5E, FI-00014 Helsinki, Finland
[g] HiLIFE – Helsinki Institute of Life Science, University of Helsinki, FI-00014 Helsinki, Finland
[h] CESPU – Instituto de Investigação e Formação Avançada em Ciências e Tecnologias da Saúde, Rua Central de Gandra 1317, 4585-116 Gandra, Portugal

ARTICLE INFO

Keywords:
Nanoparticles
Human immunodeficiency virus
Microfluidic production
Targeting
Blood-brain barrier

ABSTRACT

The human immunodeficiency virus (HIV) uses the brain as reservoir, which turns it as a promising target to fight this pathology. Nanoparticles (NPs) of poly(lactic-co-glycolic) acid (PLGA) are potential carriers of anti-HIV drugs to the brain, since most of these antiretrovirals, as efavirenz (EFV), cannot surpass the blood–brain barrier (BBB). Forasmuch as the conventional production methods lack precise control over the final properties of particles, microfluidics emerged as a prospective alternative. This study aimed at developing EFV-loaded PLGA NPs through a conventional and microfluidic method, targeted to the BBB, in order to treat HIV neuropathology. Compared to the conventional method, NPs produced through microfluidics presented reduced size (73 nm *versus* 133 nm), comparable polydispersity (around 0.090), less negative zeta-potential (−14.1 mV *versus* −28.0 mV), higher EFV association efficiency (80.7% *versus* 32.7%) and higher drug loading (10.8% *versus* 3.2%). The microfluidics-produced NPs also demonstrated a sustained *in vitro* EFV release (50% released within the first 24 h). NPs functionalization with a transferrin receptor-binding peptide, envisaging BBB targeting, proved to be effective concerning nuclear magnetic resonance analysis ($\delta = -0.008$ ppm; $\delta = -0.017$ ppm). NPs demonstrated to be safe to BBB endothelial and neuron cells (metabolic activity above 70%), as well as non-hemolytic (1–2% of hemolysis, no morphological alterations on erythrocytes). Finally, functionalized nanosystems were able to interact more efficiently with BBB cells, and permeability of EFV associated with NPs through a BBB *in vitro* model was around 1.3-fold higher than the free drug.

1. Introduction

Human immunodeficiency virus (HIV) infection and acquired immunodeficiency syndrome (AIDS) belong to a spectrum of conditions derived from the HIV. The virus-associated pathology is characterized by a neurovirulent profile, thus being able to infect the brain, using this site as reservoir, and cause severe central nervous system (CNS) damage [1]. In consequence, CNS is recognized as a sanctuary site for virus replication.

The CNS is a well-protected structure by means of biological barriers, namely the blood-brain barrier (BBB). This barrier, which is mainly formed by endothelial cells that line cerebral microvessels, plays a key role in the maintenance of a precisely regulated CNS microenvironment [2]. However, the same mechanisms that protect this complex physiological system against dangerous compounds can also avoid brain-targeted drug delivery to be effective [3].

Efavirenz (EFV) is an antiretroviral drug, approved by Food and Drug Administration (FDA) for HIV infection treatment [4], which acts by attaching and blocking a virus-specific enzyme, the reverse transcriptase [5–7]. However, in the case of EFV and other antiretroviral drugs, the final amount of drug that reaches CNS is only a small fraction of the administered dose, due to their poor ability to cross the BBB [8]. Besides hindering the therapeutic effect, this may involve the interaction of drug molecules with healthy tissues, even causing the loss of

* Corresponding author at: i3S – Instituto de Investigação e Inovação em Saúde, Universidade do Porto, Rua Alfredo Allen 208, 4200-135 Porto, Portugal.
E-mail address: bruno.sarmento@ineb.up.pt (B. Sarmento).

https://doi.org/10.1016/j.ejpb.2018.01.014
Received 16 December 2017; Received in revised form 18 January 2018; Accepted 24 January 2018
Available online 31 January 2018
0939-6411/

drug efficacy and the emergence of undesirable effects [9].

The drawback faced by drugs when it comes to BBB crossing can be circumvented by formulating them into an appropriate drug delivery system (DDS). Nanoparticles (NPs) are considered one of the most auspicious DDSs into regions of difficult access, like the brain, being able to provide protection to therapeutic agents while efficiently delivering them into the damaged areas [10–13]. Moreover, NPs offer the opportunity of being functionalized with specific ligands, hence providing an accurate targeting to the biological site of interest. Nowadays, polymeric NPs are most of the times preferred as DDSs due to their favorable properties for drugs loading and delivery. Particularly in this field, poly(lactic-co-glycolic acid) (PLGA) has shown immense potential [14]. Already considered the Holy Grail among the synthetic polymers to be applied in the biomedical field, PLGA is a FDA-approved polymer, attractive regarding its properties of versatility, biocompatibility and biodegradability [15].

Among the different techniques available to produce NPs as DDSs, nanoprecipitation may be used to encapsulate EFV in PLGA NPs. The successful loading of drugs within these DDSs core depends on their pharmaceutical properties and particles composition, but also on the encapsulation method [23]. Techniques performed by conventional methods, using equipments as homogenizers or magnetic stirrers, offer several limitations, such as the lack of precise control over NPs final properties [16]. Therefore, microfluidic platforms emerged as potential candidates to produce drug-loaded NPs in a well-controlled process using the same techniques [17,18]. Microfluidics is a multidisciplinary field intersecting science and technology, that deals with the manipulation of nanoliter volumes of fluids in channels ranging from tens to hundreds of micrometers [19]. Microfluidics is associated with a fine manipulation of process parameters, thus providing the optimization and tunability of NPs properties, including encapsulation efficiency of drugs in the systems and monodispersity of batches. This method is able to tightly control the local particle-formation environment in a continuous flow pattern [20]. Since the production process of NPs through microfluidics is continuous, this contributes to the reduction of batch-to-batch oscillations in relation to the final properties of the nanosystems [18]. The accurate manipulation of fluids and their laminar regimen inside the microchannels lead to the preservation of controlled hydrodynamic conditions, which are rapidly defined and kept during the process of formation of particles [21,22].

This work proposes the development of a DDS based on PLGA NPs able to carry EFV to the brain, hence crossing the BBB and fighting HIV neuropathology, to be administered by the intravenous route. Nanoprecipitation technique performed through both conventional and microfluidic approaches was used to produce the NPs. After comparison of NPs final properties resulting from both methods, the most suitable to accomplish the purpose of this work was selected. After this, a functionalization strategy was implemented, involving the targeting to the BBB through a transferrin receptor-binding peptide. NPs were evaluated for their EFV *in vitro* release, cytotoxicity, hemocompatibility, interaction with BBB endothelial cells, and BBB crossing ability.

2. Materials and methods

2.1. Materials

PLGA (PLGA 5004 A) was kindly provided by Corbion (Amsterdam, Netherlands). Transferrin receptor-binding peptide (Thr-His-Arg-Pro-Pro-Met-Trp-Ser-Pro-Val-Trp-Pro) was purchased from Eurogentec (Liege, Belgium), PLGA labelled with Flamma 648 (PLGA-FKR648) from PolySciTech (West Lafayette, IN, USA), and the crosslinker (NH2-PEG-Mal, PEG of 5 kDa) from Biochempeg (Watertown, MA, USA).

Tween® 80, hydrocortisone, ascorbic acid, 4-(2-hydroxyethyl)-1-piperazineethanesulfonic acid (HEPES), basic fibroblast growth factor (bFGF), 3-(4,5-dimethylthiazol-2-yl)-2,5-diphenyltetrazolium bromide (MTT), acetic acid glacial, 2-(N-morpholino)ethanesulfonic acid (MES), 1-ethyl-3-(3-dimethylaminopropyl)carbodiimide (EDC), N-hydroxysuccinimide (NHS), Histopaque-1077, paraformaldehyde, sodium chloride, uranyl acetate, Pluronic® F-127 and sodium azide were acquired from Sigma-Aldrich (St. Louis, MO, USA); EFV from BDR Lifesciences (Vadodara, India); DMSO from VWR (West Chester, PA, USA); endothelial basal medium 2 (EBM-2) and high glucose with ultraglutamine Dulbecco's Modified Eagle medium (DMEM) from Lonza (Basel, Switzerland); acetonitrile and versene from Thermo Fisher Scientific (Waltham, MA, USA); Triton X-100 from Spi-Chem (West Chester, PA, USA); fetal bovine serum (FBS), penicillin-streotomycin, chemically defined lipid concentrate, Hank's Balanced Salt Solution (HBSS), rat tail collagen type I and acetic acid, from Gibco (Waltham, MA, USA); glutaraldehyde from AGAR Scientific (London, UK); sodium cacodylate from Fluka (Buchs, Switzerland); ethanol from Valente e Ribeiro, Lda (Lisbon, Portugal); Alexa Fluor® 546 Phalloidin from Life Technologies (Baltimore, MD, USA) and VECTASHIELD® from Vector Laboratories, Inc. (Burlingame, CA, USA). Transwell® cell culture inserts (transparent polyester membrane; 12-well plate format; 0.4 μm pore size) were purchased from Corning Inc. (Corning, NY, USA).

Immortalized human cerebral microvascular endothelial cell line (*h*CMEC/D3 cell line) was purchased from Cedarlane (Hornby, ON, Canada), and mouse neuroblastoma (N18 tg 2) × rat dorsal root ganglion neurone hybrid cell line (ND7/23 cell line) was purchased from European Collection of Cell Cultures (ECACC, Wiltshire, UK) and kindly provided by Dr. Pedro Moreno (i3S, Portugal).

2.2. Methods

2.2.1. Microfluidic platform fabrication

The microfluidic platform was assembled by gathering borosilicate glass capillaries on a glass slide, as previously described [23–25]. Briefly, the chip was composed of two cylindrical capillaries (World Precision Instruments Inc., Sarasota, FL, USA), for which the outer diameter of the tapered one fitted the inner dimensions of the other. One end of the internal capillary, comprising an inner and outer diameters of around 580 and 1000 μm, respectively, was tapered using a micropipette puller (P-97, Sutter Instrument Co., Novota, CA, USA) to a diameter of 20 μm; then, this diameter was enlarged to around 80 μm using a microforge (P-97, Sutter Instrument Co., Novota, CA, USA). This capillary was partially placed into the external one, which had an inner dimension of around 1000 μm (Vitrocom, Mountain Lakes, NJ, USA), and coaxially aligned. A transparent epoxy resin (5 min® Epoxi, Devcon, Danvers, MA, USA) was used to fix the capillaries.

2.2.2. Production of nanoparticles

The production of NPs was based on the nanoprecipitation technique performed through a conventional and microfluidic approach (Fig. 1). The organic phase consisted of a mixture of 20 mg/mL of PLGA in DMSO, containing 3 mg/mL of EFV. The aqueous phase consisted of 2% Tween® 80 solution.

Considering the conventional method of NPs production, 1 mL of organic phase was directly injected with a needle (25 G) into 20 mL of aqueous phase. Then, the mixture was left under mechanical stirring for 3 h, at 200 rpm and room temperature.

Regarding NPs production through microfluidics, the organic and aqueous phase corresponded to the inner and outer fluid, respectively. The phases were injected separately into the microfluidic platform through polyethylene tubes (Smiths Medical International Ltd., Kent, UK) attached to syringes (Henke-Sass Wolf GmbH, Tuttlingen, Germany), at constant flow rates controlled by syringe pumps. After optimization, the flow rate of the inner and outer fluid was defined as 2500 and 3750 μL/min, respectively. In the end, NPs suspension was gently vortexed.

The production of NPs was run until a final volume of around 20 mL for both methods. Unloaded (i.e., without EFV) and fluorescent NPs were prepared using the same procedure but skipping the addition of

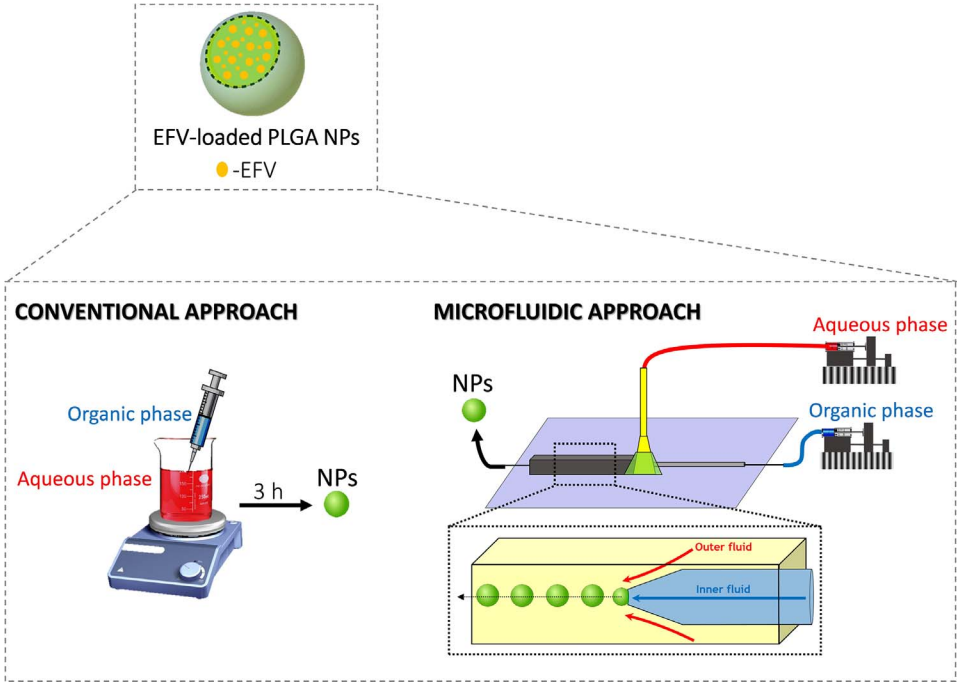

Fig. 1. Schematic representation of the conventional and microfluidic approaches used to produce EFV-loaded PLGA NPs. The organic phase consisted of a mixture of PLGA in DMSO, while the aqueous phase consisted on a solution of Tween®80.

EFV. In the case of fluorescent NPs, 10% of the PLGA used in the production of NPs consisted on PLGA-FKR648.

After production, NPs resulting from both methods of production were washed three times with ultrapure water and recovered by ultrafiltration using Amicon Ultra-15 Centrifugal Filter units (Merck Millipore, Billerica, MA, USA) with a molecular weight cutoff (MWCO) of 100 kDa.

2.2.3. Characterization of nanoparticles

2.2.3.1. Mean particle size, size distribution and surface charge. NPs were characterized for their average size (Z-average) and polydispersity index (PDI) by dynamic light scattering (DLS) and zeta-potential (ζ-potential) through laser Doppler anemometry (LDA), using a Malvern Zetasizer Nano ZS instrument (Malvern Instruments Ltd., Worcestershire, UK).

For these measurements, samples were diluted (1:100) in an ionic solution of 10 mM sodium chloride.

2.2.3.2. Association efficiency and drug loading. To determine the association efficiency (AE) and drug loading (DL) of the developed nanosystems, the amount of EFV associated to NPs was indirectly estimated. This calculation was made by the difference between the total amount of EFV used to prepare the systems and the amount of EFV that remained in the aqueous phase, after nanoparticles collection by ultrafiltration, according to Eqs. (1) and (2) [26].

$$AE\ (\%) = \frac{Initial\ mass\ of\ EFV - Mass\ of\ recovered\ EFV}{Initial\ mass\ of\ EFV} \times 100 \quad (1)$$

$$DL\ (\%) = \frac{Initial\ mass\ of\ EFV - Mass\ of\ recovered\ EFV}{Total\ mass\ of\ NPs} \times 100 \quad (2)$$

The amount of EFV was determined using a high-performance liquid chromatography (HPLC) method previously established [27]. Briefly, the quantification was performed by reversed-phase HPLC with ultraviolet detection using a Merck-Hitachi LaChrom® HPLC system (Merck, Rahway, NJ, USA). A Symmetry C8 column (5 μm, 4.6 × 250 mm; Milford, MA, USA) with LiChrospher 100 RP-18 guard column (Merck, Rahway, NJ, USA) was used as stationary phase. Chromatographic runs were performed using an isocratic method and the mobile phase used was acetonitrile:10 mM acetate buffer pH 4.0 (57:43), at a flow rate of 1 mL/min. Samples injection volume was 10 μL and the detection wavelength was at 247 nm.

2.2.3.3. Morphology and chemical screening. The morphological features of NPs were analyzed by transmission electron microscopy (TEM) with a JEOL JEM 1400 microscope (JEOL Ltd., Tokyo, Japan) at an accelerating voltage of 120 kV. The energy-dispersive X-ray spectra (EDS) were collected for chemical analysis. Images were digitally recorded using a Gatan SC 1100 ORIUS CCD camera (Gatan Inc., Warrendale, PA).

Samples were prepared by dropping 10 μL of NPs suspension onto a 300-mesh nickel grid, and stained with uranyl acetate. NPs resulting from the microfluidic method of production were prior diluted ten times in water.

2.2.4. In vitro release study

For the release study, EFV-loaded NPs (corresponding to 315 μg of drug) were added to 6 mL of 0.2% of Pluronic® F-127 in PBS solution, pH 7.4, and then placed into an orbital shaker incubator, at 100 rpm and 37 °C, during 24 h (sink conditions were assured). Aliquots of 500 μL were collected at specific time points during the assay, and the withdrawn volume was replaced with pre-heated 0.2% of Pluronic® F-127 in PBS solution. All the collected aliquots were centrifuged at 10,000*g* for 15 min and the supernatant was used for HPLC analysis, in order to quantify the EFV released from NPs over time.

2.2.5. Nanoparticles functionalization and characterization

2.2.5.1. Functionalization process. PLGA NPs were functionalized with a transferrin-receptor binding peptide. A carbodiimide coupling chemistry was performed, where the carboxyl groups of PLGA (–COOH) were conjugated with the amine groups of a PEG-based crosslinker, NH_2-PEG-Mal. Then, a maleimide coupling chemistry was run in order to conjugate the maleimide group of the crosslinker (-Mal) with the terminal cysteine of the peptide through its sulfhydryl group (-SH).

Regarding the carbodiimide reaction, 1 mg/mL of NPs was dispersed in MES solution (10 mM, pH = 5.5) containing 1 mol of EDC and 0.5 mol of NHS for each mol of carboxyl groups of PLGA, as well as 3 μg/mL of crosslinker (adapted from [23,28,29]). Afterwards, the

mixture was kept stirring (300 rpm) overnight at room temperature. NPs were washed three times with ultrapure water to remove by-products of the reaction and unbound crosslinker, and were collected by ultrafiltration. Afterwards, NPs were dispersed in PBS pH 7.4, the peptide was added in a molar ratio of 1:15 in relation to the PLGA NPs, and the maleimide reaction was allowed to run for 3 h at room temperature (adapted from [28,29]). NPs were washed again to remove unbound peptide and recovered by ultrafiltration.

2.2.5.2. Nuclear magnetic resonance. To confirm the presence of the peptide after NPs functionalized, proton nuclear magnetic resonance (^{1}H NMR) spectroscopic analysis was used for the detection of differences on spectra from non-functionalized and functionalized particles. Non-functionalized and functionalized unloaded PLGA NPs, as well as commercial PLGA used in the production process of NPs, were dissolved (3 mg) in deuterated DMSO (DMSO-d_6) and placed on appropriate nuclear magnetic resonance tubes. The analysis was performed at room temperature on a Brüker AMX 300 spectrometer (Bruker, Karlsruhe, Germany) operating at 400.13 MHz, with every chemical shift value (δ) expressed relatively to tetramethylsilane (TMS) as an internal reference.

2.2.6. Cell culturing

Both *h*CMEC/D3 and ND7/23 were grown in tissue culture flasks (passage 38–50 and 11–21, respectively). The *h*CMEC/D3 cell line was maintained in EBM-2 media supplemented with FBS (5%, v/v), penicillin-streptomycin (1%, v/v), hydrocortisone (1.4 μM), ascorbic acid (5 μg/mL), chemically defined lipid concentrate (1/100, v/v), HEPES (10 mM) and bFGF (1 ng/mL). This last supplement was added extemporaneously in the culture medium.

The ND7/23 cell line was maintained in DMEM supplemented with FBS (10%, v/v) and penicillin-streptomycin (1%, v/v). Cell cultures were kept in an incubator (CellCulture CO_2 incubator, ESCO GB Ltd., Downton, UK) at 37 °C with 5% CO_2, in a water saturated atmosphere. Cell culture medium was changed every 2–3 days.

2.2.7. Cellular metabolic activity assay

Samples toxicity was assessed in the *h*CMEC/D3 and ND7/23 cell lines using the MTT metabolic viability assay. For the *h*CMEC/D3 cell line, 200 μL of cells were seeded in a 96-well plate in a concentration of 0.04×10^6 cells/mL in EBM-2 [29]. Regarding the ND7/23 cell line, the same volume was seeded in a concentration of 0.015×10^6 cells/mL in supplemented DMEM. After the seeding, cells were incubated during 24 h and then medium was removed and cells were washed with 200 μL of PBS, pH 7.4. Thereupon, cells were incubated with free EFV, unloaded NPs, functionalized unloaded NPs, EFV-loaded NPs and functionalized EFV-loaded NPs, in concentrations of 100, 10, 1, 0.1, and 0.01 μM (in medium) determined in relation to the drug, for 24 h. Afterwards, solutions were discarded, cells were washed with 200 μL of PBS and then treated with 200 μL of MTT solution (0.5 mg/mL, in medium), during 4 h in the dark. Formazan crystals, resulting from the reduction of MTT by viable cells, were solubilized with 200 μL of DMSO, under 20 min slight shake, at 100 rpm and room temperature. Finally, absorbance was measured at 590 and 630 nm.

A negative control (NC), consisting on cells incubated with 1% of Triton X-100 in medium solution (0% of metabolic activity), and a positive control (PC), consisting on cells incubated only with medium (100% of metabolic activity), were also prepared and treated similarly to the sample wells. Metabolic activity was expressed as a percentage compared to the controls according to the Eq. (3) [29].

$$Metabolic\ activity\ (\%) = \frac{Experimental\ value - NC}{PC - NC} \times 100 \quad (3)$$

2.2.8. Hemocompatibility assay

2.2.8.1. Quantification of hemolysis. The assay related to the quantification of hemolysis resulted from an adaptation of the protocol previously described by Pinto et al. [30]. Red blood cells were isolated from buffy coats (obtained from Immunohemotherapy Service, S. João Hospital, Porto, Portugal). Briefly, 2 mL of the buffy coat content were centrifuged over density gradient with 2 mL of Histopaque-1077 for 30 min at 400*g* and room temperature, in accordance with the instructions of the manufacturer. After removal of the plasma upper layer, the lower layer containing red blood cells was washed three times with 8 mL of PBS, pH 7.4 (centrifugations for 30 min at 400*g* and room temperature). Then, 100 μL of red blood cells in a concentration of 2×10^8 cells/mL were placed in *eppendorf* tubes. Next, 100 μL of free EFV, unloaded NPs, functionalized unloaded NPs, EFV-loaded NPs and functionalized EFV-loaded NPs were added to the tubes to obtain a final concentration of 50, 5, 0.5, 0.05, and 0.005 μM in PBS (concentrations determined in relation to the drug). *Eppendorf* tubes were incubated for 3 h at 100 rpm and 37 °C. Afterwards, tubes were centrifuged at 400*g* for 5 min to collect the supernatants, which were transferred (80 μL) to 96-well plates for absorbance reading.

The PC, consisting on cells incubated with 1% of Triton X-100 (100% hemolysis), and NC, consisting on cells incubated only with PBS (0% hemolysis), were also prepared and treated similarly to the sample tubes.

The hemoglobin value of the samples was calculated in accordance with Eq. (4) [30].

$$Hemoglobin\ value\ of\ sample\ (\mathrm{mg/dL}) = \frac{[2 \times A_{415} - (A_{380} + A_{450})] \times 100 \times D_f}{E} \times 100 \quad (4)$$

where A_{380} is the absorbance value at 380 nm, A_{415} is the absorbance value at 415 nm, A_{450} is the absorbance value at 450 nm, D_f is the dilution factor (that was 35), and E is the molar absorptivity of oxyhemoglobin at 415 nm (that is 79.46). The absorbance value at 415 nm corresponds to the Soret band absorption of hemoglobin, and the absorbance values at 380 and 450 nm correspond to the absorption of uroporphyrin, which falls under the same wavelength range.

Afterwards, the hemolytic potential of the samples was calculated in accordance with Eq. (5) [30].

$$Hemolysis\ (\%) = \frac{Hemoglobin\ value\ of\ sampe}{Hemoglobin\ value\ of\ PC} \times 100 \quad (5)$$

The osmolarity of the formulations incubated with red blood cells were also determined at room temperature using a Micro-Osmometer M3320 (Advanced Instruments, Inc.).

2.2.8.2. Morphology of red blood cells. The assay related to the assessment of cell membrane integrity and morphology of red blood cells resulted from an adaptation of the protocol previously described by Shahbazi et al. [31] and was based on scanning electron microscopy (SEM) imaging. Briefly, after the isolation of red blood cells from buffy coats, as described for the quantification of hemolysis, 1 mL of red blood cells in a concentration of 4×10^5 cells/mL in HBSS were seeded in 6-well plates containing plastic tissue culture coverslips of 13 mm. Then, NPs dispersed in HBSS were added to the wells, to reach a final concentration of 50 μM of EFV. The plates were placed in an orbital shaker incubator for 3 h at 37 °C and 100 rpm.

NC, consisting on cells incubated only with HBSS (0% hemolysis), was also prepared and treated similarly to the sample wells.

Cells were then fixed in 2.5% glutaraldehyde in sodium cacodylate buffer (pH 7.4) for 1 h, and dehydrated in increasing concentrations of 50, 70, and 100% of ethanol for 5, 20, and 15 min, respectively. Finally, coverslips were removed from wells, mounted on SEM supports using double sided carbon adhesive tape and coated with gold/platinum under vacuum for 90 s, with a 15 mA current. Afterwards, they were observed under SEM (FEI Quanta 400F, FEI Company, Hillsboro, OR, USA) using an electron beam intensity of 10 kV and magnification

ranging from 1000 to 15,500 times.

2.2.9. Cell-nanoparticle interaction

2.2.9.1. Flow cytometry. *h*CMEC/D3 cells were detached from culture flasks with versene in order to preserve the transferrin receptor, and washed with PBS, pH 7.4. After being fixed in 0.1% sodium azide and 1% FBS in PBS (1×10^6 cells/mL, 30 min), 100 µL of cells were seeded in round-bottom 96-well plates and recovered through centrifugation at 300*g* during 7 min. Cells were ressuspended in 50 µL of non-functionalized or functionalized fluorescent NPs (400 µg/mL, in 10 mM HBSS-HEPES) and incubated for 3 h in ice. After incubation, cells were washed twice with PBS and placed in cytometer tubes.

A competition assay was performed by incubating cells with the transferrin receptor-binding peptide (50 µL at concentration of 1 mg/mL for 30 min) before adding the functionalized NPs. A control based only on cells without NPs was also performed.

The quantification of the NPs associated to the BBB endothelial cells was done using a FACS CANTO II cytometer (BD Biosciences, San Jose, CA, USA), where NPs were detected through the allophycoerythrin (APC) channel. The results were analyzed using the software FlowJo vX.0.7 and expressed as the medium fluorescence intensity (MFI).

2.2.9.2. Confocal laser scanning microscopy. The procedure for confocal laser scanning microscopy resulted from an adaptation of the protocol previously described by Gomes et al. [29]. *h*CMEC/D3 cells were seeded in glass coverslips of 14 mm (400 µL at concentration of 2.5×10^5 cells/mL), placed inside a 24-well plate and pre-coated with type I collagen for 1 h, and were allowed to attach overnight. Cells were washed twice with PBS pH 7.4, and then 200 µL of non-functionalized or functionalized fluorescent NPs (400 µg/mL, in 10 mM HBSS-HEPES) were added to each well and incubated for 3 h at 37 °C. After incubation, cells were washed twice with PBS, fixed with PFA 4% (200 µL) for 7 min, washed again three times with PBS (2 min each), and permeabilized with 0.1% Triton X-100 for 10 min (200 µL). After a new washing step, actin-network was labelled with Alexa Fluor® 546 Phalloidin (1:200, 200 µL) for 20 min. The excess of staining solution was washed three times with PBS. Finally, coverslips were mounted on a slide using VECTASHIELD® mounting medium for subsequent microscopic observation.

A competition assay was performed by incubating the cells with the transferrin receptor-binding peptide (200 µL at a concentration of 1 mg/mL for 30 min) before adding the functionalized NPs.

The interaction between nanoparticles and brain endothelial cells was assessed through a confocal microscope (Leica Microsystems GmbH, Wetzlar, Germany).

2.2.10. Permeability study

The guidelines to set up the BBB *in vitro* model used in the permeability study were already reported in previous works [28,32]. Briefly, 2.5×10^4 cells/cm^2 of *h*CMEC/D3 cells (500 µL of medium) were seeded on 12-Transwell® cell culture inserts (apical side). Previously to the seeding, the inserts were coated with 90 µL of a 50 µg/mL rat tail collagen type I in acetic acid solution (0.02 M) for 1 h, at 37 °C, and then washed twice with PBS pH 7.4. The basolateral side was filled with 1.5 mL of medium. The system was maintained in the incubator at 37 °C with 5% CO_2 during 8 days, and medium was changed every 2 days. The *h*CMEC/D3 cells monolayer became confluent at the day 8 after seeding, which was the day appropriate to perform the permeability study. The integrity of the cell monolayer was checked every 2 days by monitoring the transendothelial electric resistance (TEER) using an endothelial Volt–Ohm meter (Millicell® ER S-2; Merck Millipore, Billerica, MA, USA). The resistance value of an empty filter was subtracted from each measurement.

The permeability experiment was performed in the apical-to-basolateral direction. After removing the cell culture medium, the basolateral compartment was filled with 1.5 mL of 0.2% Pluronic® F-127 in HBSS, ensuring sink conditions. Regarding the apical compartment, 500 µL of EFV 10 µM, in the free form or loaded on PLGA NPs, diluted in HBSS were added. Then, the assay was conducted at 37 °C using an orbital shaker incubator (100 rpm). At different time points (15, 30, 45, 60, 90 and 120 min), 200 µL samples were taken from the basolateral side, and the same volume of pre-heated 0.2% Pluronic® F-127 in HBSS was added to replace the withdrawn volume. The integrity of the cell monolayer was checked during the permeability experiment by monitoring the TEER.

All samples were used for HPLC analysis, in order to quantify EFV.

2.2.11. Statistical analysis

All the results were represented as mean ± standard deviation from a minimum of three independent experiments. Statistical analysis was performed by one-way analysis of variance (ANOVA) followed by a post hoc test (Tukey's honestly significant difference) to compare more than two groups. In case of comparison of two different groups, unpaired Student *t*-test was used.

Differences were considered significant at $p < 0.05$, $p < 0.01$, or $p < 0.001$. All statistical analysis was performed with the software GraphPad Prism 5 (GraphPad Software Inc., San Diego, CA, USA).

3. Results and discussion

3.1. Conventional and microfluidic production: Comparison of nanoparticles properties

The development of NPs was based on the nanoprecipitation technique performed through both the conventional and microfluidic method of production.

The co-flow geometry of the fluids was adopted in the production of NPs through microfluidics. This geometry implied that the inner fluid flowed inside the internal capillary, while the outer fluid flowed between the internal and external capillaries, in the same direction [33]. Following co-flow in parallel directions and merger of fluids from the tapered end of the internal capillary, they underwent turbulence-free mixing by well-defined diffusion of molecules across the interface between the organic and aqueous phase, subsequently leading to the formation of nanoparticulate systems [34,35].

The final properties of NPs were compared between the two methods of production, in order to understand which of them could be more fruitful concerning the aim of the work.

Table 1
Properties of NPs resulting from the conventional and microfluidic approach. Results are presented as mean ± SD ($n = 3$).

Method	NPs	Z-average (nm)	PDI	ζ-Potential (mV)	AE (%)	DL (%)
Conventional	Unloaded	134.0 ± 2.7	0.092 ± 0.009	−27.4 ± 3.1	–	–
	EFV-loaded	133.0 ± 3.6	0.090 ± 0.010	−28.0 ± 2.4	32.7 ± 1.0	3.2 ± 0.1
Microfluidic	Unloaded	70.9 ± 3.2***	0.085 ± 0.003	−15.0 ± 1.6**	–	–
	EFV-loaded	72.8 ± 4.9	0.086 ± 0.004	−14.1 ± 1.3	80.7 ± 8.3	10.8 ± 1.1

Z-average: average size; PDI: polydispersity index; ζ-Potential: zeta-potential; AE: association efficiency; DL: drug loading; NPs: nanoparticles; EFV: efavirenz.
** and *** denote a significant difference of $p < .01$ and $p < .001$, respectively (comparison between unloaded and EFV-loaded NPs resulting from both methods).

The results for the evaluation of the obtained NPs in relation to their Z-average, PDI, and ζ-potential were depicted in Table 1. All formulations presented NPs which met the requirement of a Z-average under 200 nm, which is important to accomplish the brain-targeted drug delivery [36]. The size of NPs obtained by microfluidics (around 70 nm) was significantly lower ($p < 0.001$) compared to the conventional methodology (around 133 nm). It is well known that lower sizes of NPs enable longer blood half-time [37]. Moreover, Gao et al. injected polymeric drug-loaded NPs with sizes of 70, 170, 220 and 345 nm into rats (at the same dose), and proved that NPs with a size smaller than 100 nm led to the highest drug level in the brain; the authors associated the size of 70 nm with an easier endocytosis of NPs by vascular endothelial cells of the BBB [38]. Compared to the conventional production, the mixing in microfluidic platforms is usually faster than the time necessary to occur NPs nucleation and growth. Therefore, the polymer is not able to adsorb to recently-formed NPs, and ends up forming more particles with a smaller size [18,39]. In relation to PDI of NPs, results were not significantly different between the different approaches. However, it is necessary to highlight that the microfluidic technology was able to provide PDI values as low as the ones obtained by the conventional methodology (around 0.1). This was expected since particles narrow size distribution is commonly associated with microfluidic technology [40]. Regarding ζ-potential, results demonstrated a significant increase in surface charge ($p < 0.001$) when performing NPs production by microfluidics, instead of the conventional methodology. This may be explained by an increase in the quantity of Tween®80 associated with the particles when they were produced using the microfluidic approach, hence retaining a less negative charge [41]. Still, all formulations presented a negative ζ-potential, which is due to the end carboxyl groups of PLGA [42]. Unloaded and EFV-loaded NPs presented similar properties in relation to the mentioned physical-chemical parameters.

Microfluidics-associated AE of NPs was significantly higher (around 80%; $p < 0.001$) compared to the conventional methodology, with a difference of around 50%. Moreover, DL experienced a significant increase ($p < 0.001$) in microfluidics-produced NPs (around 11%) in comparison to the conventional method (around 3%). Liu et al. attributed AE and DL differences between the two methods to the fixed higher volume ratio between the aqueous and organic phase in microfluidics, instead of a gradual increase in the ratio of these two phases during the conventional NPs synthesis process [43]. Moreover, it is probable that a slower solvent diffusion in microfluidics might promote less simultaneous drug migration out of the particles during the fabrication process, creating a coefficient which did not favor EFV presence in the aqueous phase. This is in accordance with the work of Luo et al. [18], who referred that microfluidics reduces the movement of molecules from the organic to the aqueous phase, hence promoting the effectiveness of drug entrapment. Moreover, the reduced drug loss due to fewer steps involved in microfluidics-assisted NPs production compared to sequential conventional mixing of phases may contribute to the difference observed between the two methods concerning AE and DL of particles [44]. The selected combination of inner and outer flow rates allowed matching drug flow with nanosystems generation and that the population of PLGA NPs were formed from the tapered end of the internal capillary under precisely the same conditions, including drug/polymer and surfactant concentration, thus contributing to a better EFV entrapment [34]. NPs formulations associated with low AE and DL values imply the administration of large amounts of non-therapeutic excipients to reach a clinically relevant drug dose, which is associated with side effects emergence [45,46]. Thus, these two parameters are of extreme importance when developing DDSs.

TEM analysis (Fig. 2) revealed round-shaped particles with relatively smooth surfaces. Moreover, no apparent morphological differences were found between NPs resulting from the two production methods. According to the images, PDI of NPs resulting from both methods demonstrated to be similar, which corroborated DLS data.

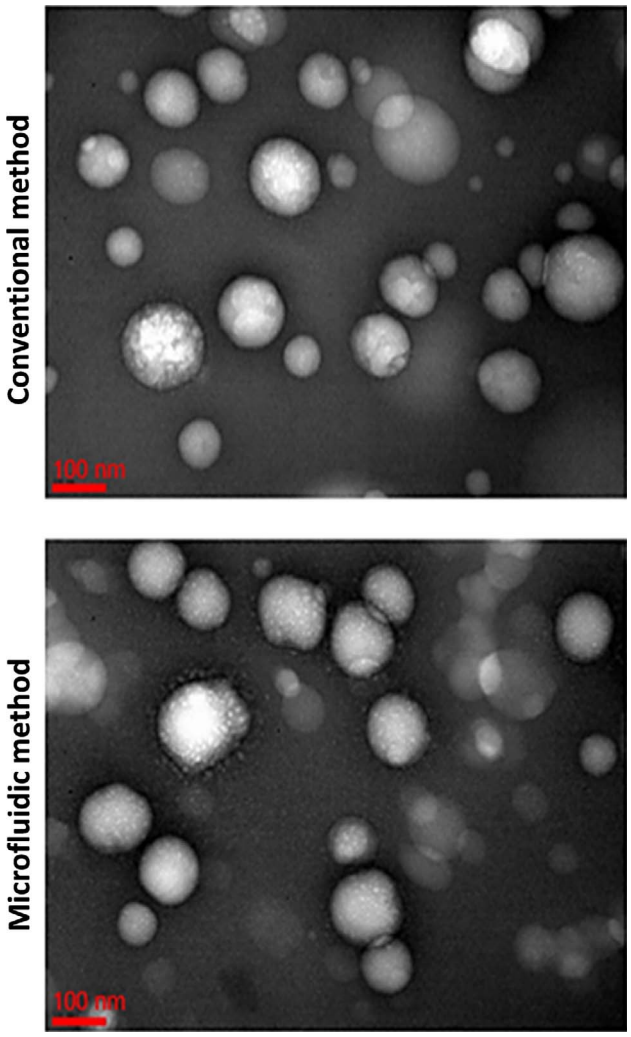

Fig. 2. TEM images of EFV-loaded PLGA NPs produced by the conventional and microfluidic method.

Regarding particles size, TEM images of microfluidics-produced NPs showed a discrepancy compared to DLS measurements. However, TEM only provides a visualization of a limited number of NPs, while DLS allows to averagely estimate the size of several thousands [47]. Therefore, DLS results may be considered more reliable, since it is a more quantitative technique, hence providing an overview of the whole sample.

The EDS capability of TEM was used for elemental mapping of EFV-loaded PLGA NPs produced through both conventional and microfluidic method (Table 2). Since the microfluidic method implied considerable higher volume of DMSO involved on the production of each batch of NPs compared to the conventional one, the need for evaluating the

Table 2
EDS analysis of EFV-loaded PLGA NPs produced through both conventional and microfluidic method. Results are presented as mean ± SD ($n = 5$).

Element	Associated substance	Method of NPs production	Average atomic (%)
S	DMSO	Conventional	0.04 ± 0.02
		Microfluidic	0.02 ± 0.03
F	EFV	Conventional	0.15 ± 0.10
		Microfluidic	0.37 ± 0.07*

S: sulfur; F: fluorine; DMSO: dimethyl sulfoxide; NPs: nanoparticles; EFV: efavirenz.
* denotes a significant difference of $p < .05$ (comparison between each associated substance group).

amount of organic solvent remaining on their structure emerged. Moreover, EDS analysis was also useful to report the quantity of EFV associated with each NPs type, microfluidic- or conventionally-produced. Therefore, the analysis was conducted through detection of sulfur (S) and fluorine (F), which are chemical components of DMSO and EFV, respectively. A single NP was focused, scanned and analyzed for its elemental composition. As expected, the results confirmed the presence of the chemical components carbon and oxygen in all formulations of NPs, resulting from the presence of the polymer and the surfactant used in the production process. In relation to the S element, no differences in the DMSO content were found between the two methods of fabrication, evidencing that the microfluidic production did not imply an increase in the amount of organic solvent associated with the NPs. This may be considered a great achievement since organic solvents should be present in reduced amounts in the final pharmaceutical product due to their capability of raising toxicity phenomena, as well as causing changes on the organoleptic properties of the formulations [48]. In relation to the F, a significant difference ($p < 0.01$) was observed between NPs produced by the two methods. The microfluidic method allowed the formation of NPs with detectable levels of F approximately two times higher than the conventional method. This is in good accordance with the results obtained for the AE and DL of the formulations, revealing the successful association of EFV with NPs when using the microfluidic method of production.

Data obtained until this point suggested that the microfluidic method of NPs production could be advantageous, providing adequate particles size to allow BBB crossing, monodisperse batches and higher efficiency in what concerns NPs-drug association. Furthermore, some advantages inherent to the microfluidics technology needed to be stressed out, as it is far more fast, user-friendly and easy to handle compared to the conventional method of production. Thus, the microfluidics-produced formulation was selected to proceed with the next experiments, involving NPs biological characterization and functional targeting.

3.2. In vitro release assay

The release profile of EFV from microfluidics-produced PLGA NPs (Fig. 3) was characterized by an initial rapid burst effect, with around 30% of the drug being recovered from the medium in the first 30 min. This could result from the amount of drug which was near or attached to particles surface [49]. Oppositely, the amount of drug which is contained within the NPs core is usually released during a more prolonged period of time. PLGA NPs provided a release of EFV of around 50% within the first 24 h. This release behavior of drugs from PLGA NPs was frequently reported in the literature [50–53]. The mechanism responsible for the release of EFV could be pointed out as a result of the diffusion of the drug through the PLGA, and also polymer surface or bulk degradation, erosion, and swelling [54]. PLGA nanosystems were able to present a sustained release behavior, which may be due to its very well compacted internal structure, hence avoiding water penetration from the medium and promoting a relatively low drug diffusion out of NPs [55].

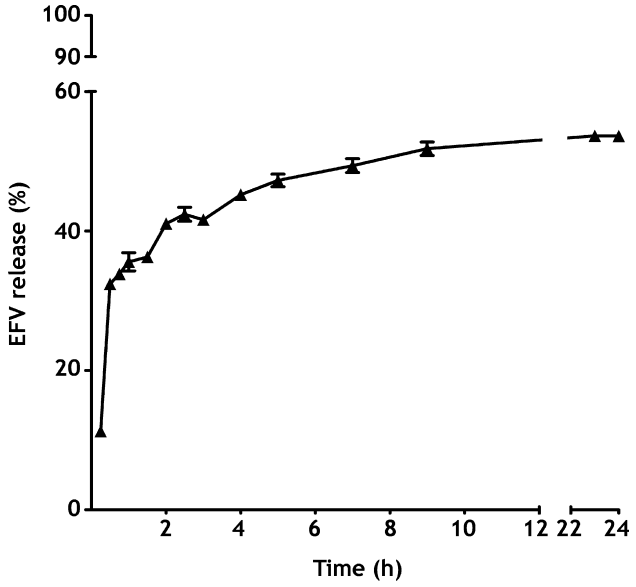

Fig. 3. *In vitro* release profile of EFV from microfluidics-produced PLGA NPs.

3.3. Nanoparticles functionalization and characterization

Nanoparticles were functionalized with a peptide-binding transferrin receptor in order to target the BBB, avoid EFV-related side effects and enhance therapeutic efficacy of the drug. In healthy conditions, this receptor is overexpressed at the BBB level, specifically in brain capillaries, which turns it as a promising mediator for drug delivery to the brain [56].

The functionalization process (Fig. 4**A**) involved two different coupling chemistries. The first one, a carbodiimide reaction, was run in order to link the carboxyl groups of PLGA to the amine groups of a PEG-based crosslinker (NH_2-PEG-Mal). This step also involved the PEGylation of NPs, which is especially important when NPs are intravenously administered, since PEG is responsible for hindering the adsorption of opsonins to the nanosystems and their consequent clearance through the phagocytic system, hence prolonging their circulation time [15,57]. The second coupling chemistry, a maleimide reaction, was used to attach the maleimide group of the PEG-based crosslinker to the terminal cysteine of the peptide. This functionalization rendered the peptide a site-orientation, due to the high specificity degree towards the coupling between the functional group of PLGA NPs (–COOH) and the one of the peptide (–SH); the linkage between them was indirectly performed, but in a specific manner, through the crosslinker. Once the NPs were functionalized, they should be theoretically able to reach the brain, mainly by interconnection with the transferrin receptor at the BBB.

A close observation of the functionalized PLGA NPs ^{1}H NMR spectra (Fig. 4B and C) allowed the confirmation of the presence of small peaks at -0.008 and -0.017 ppm, which are described in the literature as traces of the presence of the peptide, being related with the alkyl protons of its amino acids residues [29,58]. It was also possible to observe peaks at 1.4 (3H), 4.8 (2H) and 5.2 (1H) ppm which were related to the $–CH_3$, $–CH_2$, and –CH protons of PLGA, respectively [59]. In addition, an intense peak related with Tween®-80 used in NPs preparation appeared at 3.6 ppm [58].

3.4. Influence of nanosystems on cellular metabolic activity

In vitro cell viability determination was assessed through a MTT assay in the *h*CMEC/D3 (Fig. 5) and ND7/23 (Fig. 6) cell lines. The *h*CMEC/D3 cell line was chosen since brain endothelial cells represent the major cellular component of the BBB, while ND7/23 cells were used as a model of a sensorial neuron cell line of brain parenchyma. A range of concentrations from 0.01 μM to 100 μM of free EFV, unloaded NPs, functionalized unloaded NPs, EFV-loaded NPs, and functionalized EFV-loaded NPs were tested (concentration in relation to the drug).

Metabolic activity of BBB endothelial cells and neuron cells was found to be always above 90% and 70%, respectively, when in contact with all NPs, at all evaluated concentrations. Therefore, NPs formulations should be considered non-toxic, and potentially safe, according to the 10993-5 norm stated by the International Organization for Standardization (ISO), in the context of the pre-clinical testing evaluation of the cytotoxicity of medical devices by *in vitro* techniques [60].

The concentration of 100 μM free EFV demonstrated to cause severe

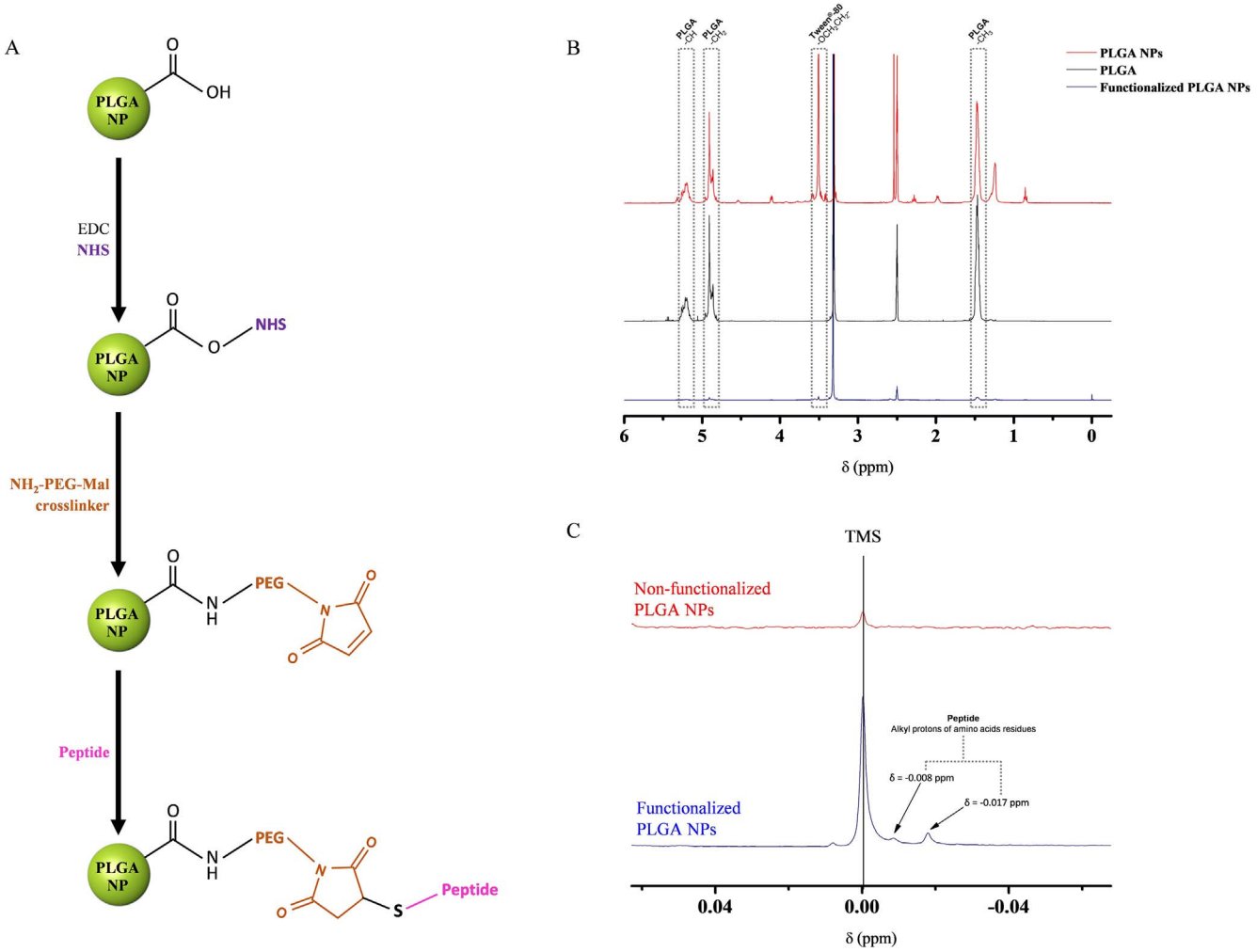

Fig. 4. (A) Functional groups of NPs during the different stages of functionalization process. (B) ^{1}H NMR spectra (DMSO-d_6) of commercial PLGA, functionalized and non-functionalized PLGA NPs at 400 MHz. (C) ^{1}H NMR analysis of both nanoparticulate systems near to 0.00 ppm, where peaks at −0.008 and −0.017 ppm are visible and described as traces of the presence of the transferrin receptor-binding peptide. Peak at 3.3 ppm is related with water presence in samples.

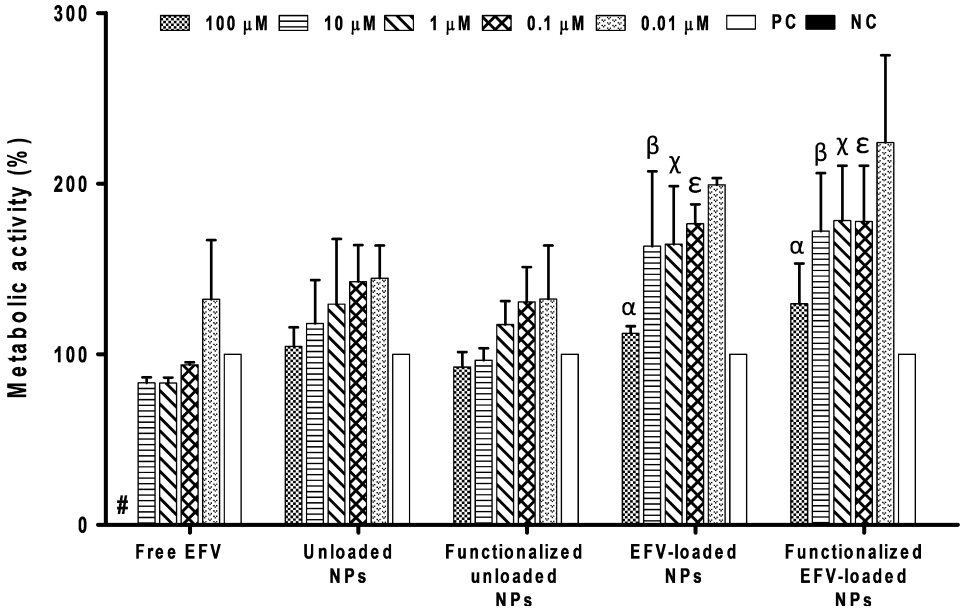

Fig. 5. Metabolic activity of *h*CMEC/D3 cells when incubated with different concentrations of free EFV, unloaded NPs, functionalized unloaded NPs, EFV-loaded NPs, and functionalized EFV-loaded NPs, during 24 h. # denotes a significant difference between free EFV 100 µM and the other concentrations in the same group. Both EFV-loaded or functionalized EFV-loaded NPs groups were compared with free EFV one, being α, β, χ and ε related with a significant difference of $p < .001$, $p < .05$, $p < .05$ and $p < .05$, respectively (comparison between equal concentrations). NC and PC consisted on cells incubated with 1% of Triton X-100 in medium, and only with medium, respectively.

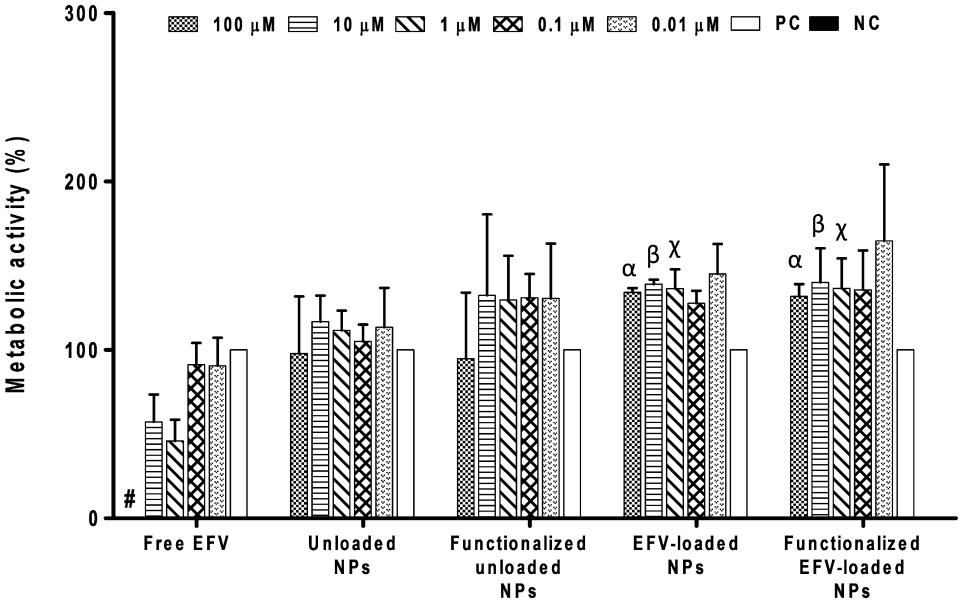

Fig. 6. Metabolic activity of ND7/23 cells when incubated with different concentrations of free EFV, unloaded NPs, functionalized unloaded NPs, EFV-loaded NPs, and functionalized EFV-loaded NPs, during 24 h. # denotes a significant difference between free EFV 100 µM and the other concentrations in the same group. Both EFV-loaded or functionalized EFV-loaded NPs groups were compared with free EFV group, being α, β and χ related with a significant difference of $p < .001$, $p < .01$ and $p < .01$, respectively (comparison between equal concentrations). NC and PC consisted on cells incubated with 1% of Triton X-100 in medium, and only with medium, respectively.

damages to both cell types, resulting in the total absence of metabolic activity. According to the obtained results, the maximum concentration limit for a safe use of the free drug form in the *h*CMEC/D3 and ND7/23 cell line is probably defined between 10 µM and 100 µM, and 1–0.1 µM, respectively.

The results for the cellular metabolic activity related to unloaded NPs (> 90%) for both cell types, reinforced the apparent low contribution of particles matrix to the emergence of cytotoxicity phenomena.

Significant metabolic activity differences can be observed when comparing equal concentrations between free EFV and EFV-loaded NPs group. The EFV-loaded NPs provided a higher cellular metabolic activity than the free drug and, therefore, it is possible to state that the cellular cytotoxicity associated with free EFV can be diminished by encapsulating the drug in NPs, demonstrating that these nanocarriers have a protective role for EFV administration in the selected *h*CMEC/D3 and ND7/23 cell lines. Moreover, functionalized EFV-loaded NPs demonstrated to have metabolic activity profiles similar to EFV-loaded NPs, indicating that the functionalization process with a peptide did not influence the safety of the nanosystems.

In general, it was possible to denote that the neuron cell line was prone to present smaller values of cellular metabolic activity in comparison to the endothelial cell line. This may be mainly due to one of the principal EFV metabolites, namely, 8-hydroxy-efavirenz, which was already associated with cytotoxicity to neuron cultures [61]. However, once again, this reduction in the cellular metabolic activity was attenuated by the encapsulation of EFV in NPs, which potentially minimized the toxic effect of the drug in the neuron cell line.

3.5. Nanoparticles hemocompatibility

Erythrocytes are the most abundant cells in the bloodstream, and they may experience deformation or membrane damages derived from intravenous-administered pharmaceutical formulations [31]. Herein, the free drug and all types of NPs formulations were directly incubated with erythrocytes in concentrations ranging from 0.005 µM to 50 µM (concentration in relation to the drug). The results for hemolysis are shown in Fig. 7.

The percentage of hemolysis for all samples at all analyzed concentrations was always below 2%, which corresponded to hemoglobin concentrations between 2.1 and 3.7 mg/dL, and no significant differences were found between the different groups. Moreover, the percentage of hemolysis calculated for the NC (0%) and PC (100%) were correlated with hemoglobin concentration of 0.1 mg/dL and 209.5 mg/dL, respectively. The obtained results demonstrated that neither the free drug, nor unloaded NPs, nor drug-loaded NPs can be considered dangerous for red blood cells. Herein, functionalized NPs demonstrated to have a hemolytic profile similar to the non-functionalized NPs, and thus the functionalization process did not affect the hemocompatibility of the nanoformulations. In accordance to a guidance for *in vitro* hemolysis described by representatives of the Johnson & Johnson and Novartis Pharmaceuticals Corporation [62], hemolysis percentages below 10% are related with non-hemolytic formulations, while hemolysis percentages above 25% are related with hemolytic formulations. Thus, the nanosystems herein developed were considered non-hemolytic. The osmolarity of the formulations was also measured (considering that PBS and blood hold similar osmolarities), in order to understand the relation between their osmotic concentration and the osmotic concentration of blood. All formulations presented osmolarity values within the range for blood osmolarity, which is 285–300 mOsm/L [63], and thus osmolarity-related hemolysis was not expected to occur.

The morphology of erythrocytes after interaction with NPs was also evaluated by SEM imaging (Fig. 8). Herein, only the maximum concentration of unloaded NPs and EFV-loaded NPs, 50 µM, was tested. NPs demonstrated to have an impact on red blood cells similar to the NC. Therefore, no considerable morphological changes in the cells were observed.

All these findings supported the theory that the NPs formulations are hemocompatible, and therefore could be safe for intravenous administration.

3.6. Cell-nanoparticle interaction

The interaction between non-functionalized and functionalized NPs with human BBB endothelial cells was quantitatively studied through flow cytometry after 3 h incubation. Confocal microscopy was also used, hence enabling a qualitative analysis of the interaction.

Flow cytometry outcomes of all samples were expressed as MFI, as represented in Fig. 9. It was possible to observe that functionalized microfluidics-produced NPs interacted with BBB endothelial cells in higher extent than non-functionalized ones, leading to a significant higher MFI value ($p < .05$). Therefore, the peptidic functionalization of NPs towards the transferrin receptor increased the interaction and

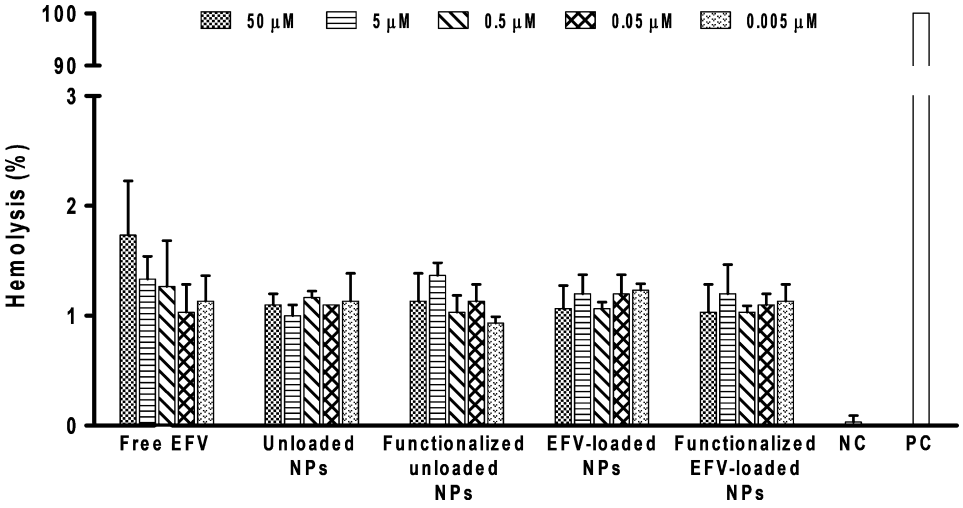

Fig. 7. Percentage of hemolysis associated with the free drug, unloaded NPs, functionalized unloaded NPs, drug-loaded NPs, and functionalized drug-loaded NPs. NC and PC consisted on cells incubated only with PBS, and with 1% of Triton X-100, respectively.

further binding to the surface and/or internalization of the nanosystems into cells. Confocal microscopy analysis (Fig. 10) also evidenced an increase in the functionalized NPs-associated fluorescence accumulated on *h*CMEC/D3 cells, compared to non-functionalized NPs. Thus, the flow cytometry and confocal microscopy study corroborated the NMR spectra outcome, and proved the achievement of a successful attachment of the peptide to microfluidics-produced PLGA NPs.

To further verify the specific role of the transferrin receptor-binding peptide used to functionalize NPs, the interaction of the functionalized nanosystems in the presence of free peptide, which acted as a competitor in what concerns receptor attachment, was also accessed. As shown in Fig. 9, the free peptide decreased the interaction between functionalized NPs and BBB endothelial cells, to levels similar to the ones found for non-functionalized NPs, thus suggesting that functionalized NPs interacted with *h*CMEC/D3 cells specifically via transferrin receptor. Exploiting this active mechanism of transport, the receptor is associated with a clathrin-mediated endocytosis. The complex ligand-receptor is captured by a clathrin-coated pit after diffusing through the plasma membrane, forming a clathrin-coated vesicle and, later on, fusing to an early endosome. The endocytosed cargo may then follow to recycling, lysosomes or other cellular pathways [28,64,65].

Confocal microscopy images (Fig. 10) supported the key role of this receptor on the interaction of functionalized NPs with the cells, demonstrating similarities between the behavior of the control (addition of free peptide prior to functionalized NPs) and non-functionalized NPs.

The results herein were in agreement with those of Gomes et al., who intended to deliver siRNA through conventionally-produced PLGA NPs, functionalized with the same peptide, in order to target the BBB

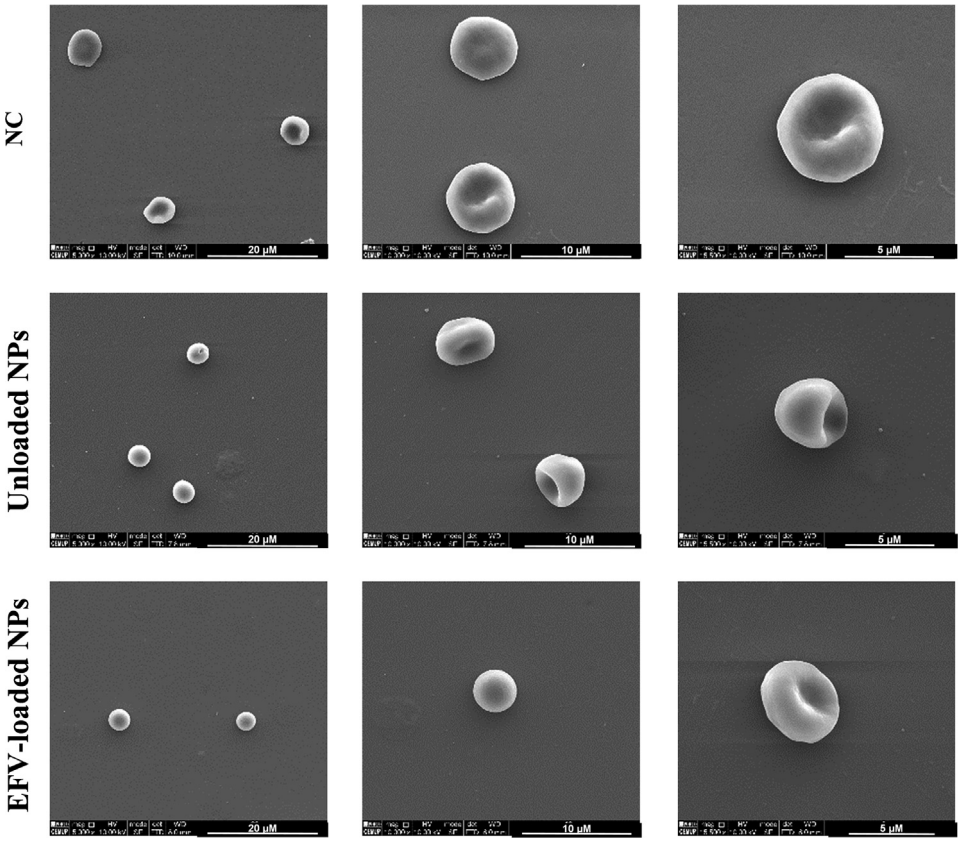

Fig. 8. SEM images of red blood cells morphology after interaction with PBS (NC), and 50 µM of unloaded NPs and EFV-loaded NPs in PBS, during 3 h. No relevant morphological differences were found between the three groups. NC consisted on cells incubated only with HBSS.

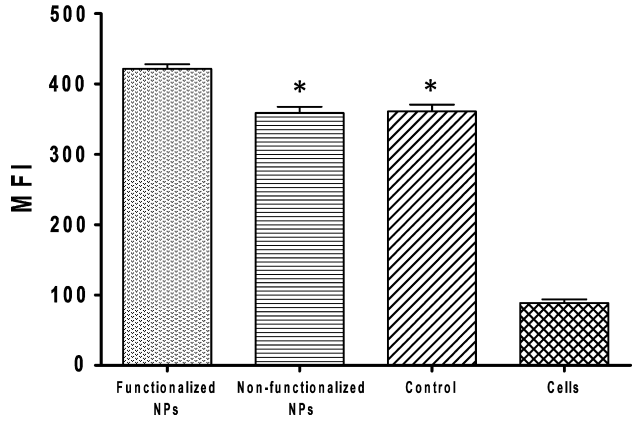

Fig. 9. The level of interaction between *h*CMEC/D3 cells and microfluidics-produced PLGA NPs, functionalized and non-functionalized, was quantified through flow cytometry (after 3 h of incubation) and reported as MFI ± SD. * denotes a significant difference ($p < .05$) when comparing NPs functionalized with a transferrin receptor-binding peptide with both non-functionalized NPs and the control, which consisted on the addition of free peptide prior to functionalized NPs (competition assay). Data ($n = 3$) illustrative of three independent experiments.

and treat CNS disorders [28,29]. The authors verified an increase in the interaction of functionalized particles with *h*CMEC/D3 cells, compared to non-functionalized ones. The site-orientation of the peptide was pointed out as a key aspect to attain a successful functionalization.

Kang and co-workers reported a nanotechnology-based product, PLGA-PEG NPs, to treat glioblastoma disease, delivering paclitaxel, and target the BBB [66]. The targeting was done through functionalization of NPs with a peptide based on an iron-mimicry moiety, driving the nanosystems to the transferrin receptor. They demonstrated an increase in the association of peptide tagged PLGA NPs with BBB endothelial cells, compared to untagged NPs, and remarkably prolonged median survival of mice treated with them.

The importance of NPs targeting to the right biological site has been more and more recognized, leading to efforts in the search for accurate functionalization processes. Herein, the functional targeting of NPs to the BBB was successfully accomplished, which represents higher probabilities of NPs accumulation in the brain and controlled biodistribution of EFV, thus ultimately leading to better outcomes on HIV-infected patients. However, further studies would be needed to be sure about the efficiency of this functionalization, for example, in what concerns NPs behavior facing protein corona phenomena.

3.7. Permeability study

Lastly, the BBB permeability of EFV was studied in order to understand to what extent the nanosystems could enhance the bioavailability of the drug across this biological barrier.

The permeability study was conducted through a cell-based BBB *in vitro* model consisting on a monolayer of *h*CMEC/D3 cells, which were allowed to grow for 8 days in a Transwell® system. TEER values within the range 40–70 Ω cm^2 were obtained, demonstrating the tightness and integrity of the cell monolayer, as verified in several transmigration studies in which the model was used [28,67–69]. In fact, recently developed BBB *in vitro* models, consisting on co-culture of different CNS cell types or primary cultures, are able to provide systems with increased complexity, resembling the *in vivo* conditions with higher precision [70]. However, they also present several disadvantages, highlighting the resemblance of *in vivo* conditions only temporarily (initial stage of development), difficult obtainment of cell sources, complex characterization, time spent in cell culture, as well as lack of reproducibility and high costs of maintenance [71,72]. Moreover, despite the simplicity, the model adopted is considered appropriate for the initial screening of drugs permeability, since *h*CMEC/D3 cells are responsible for the expression of most transporters and receptors observed in the BBB *in vivo* microenvironment [73,74].

The permeation of EFV through the BBB *in vitro* model was around 1.3-fold higher ($p < .001$) when using PLGA NPs as drug carriers (both non- and functionalized NPs), compared to the free drug, over the 120-min experimental time frame (Fig. 11). The increase in the permeability of EFV may be associated with the ability of NPs to improve the poor aqueous solubility of the drug, leading to an enhancement on its bioavailability at the BBB, and ultimately culminating in better crossing of the barrier [75,76]. This result was consistent with the work of Graverini et al., who developed a nanoparticulate system to encapsulate another poorly water-soluble drug, andrographolide, and verified an improved permeability of the nanosystem through a BBB *in vitro* model of *h*CMEC/D3 cells, compared to the free form of the compound [77].

Regarding the permeability of non-functionalized and functionalized EFV-loaded NPs, no significant differences were found between them (Fig. 11). Although the functionalization with a transferrin receptor-binding peptide demonstrated to be able to efficiently target the NPs to the BBB, providing their deposition at this biological site, it was not able to promote higher permeation of EFV through the *h*CMEC/D3 cell monolayer. However, this may be explained by the rapid recycling associated with the transferrin receptor. According to the literature, this receptor has a pre-recycling half-time of only around 10 min after internalization, which limits the transcytotic pathway and, consequently, the receptor-mediated permeation of functionalized NPs through the BBB [78,79]. Therefore, the endosomal trafficking associated with the transferrin receptor may be compromised due to the highly dynamic and transient character of the endosomes. Moreover, beyond the endosome formation during cellular internalization, the clathrin-mediated endocytosis may follow the lysosomally degradative pathway [80]. This limitation may be avoided by using ligands to functionalize NPs which promote the caveolin-mediated endocytosis through the BBB, hence escaping from the lysosomal pathway and leading to direct exocytosis of the cargo [81].

4. Conclusion

Gathering together all this knowledge, the herein work presented a profitable microfluidic method of production of EFV-loaded PLGA NPs, highlighting the smaller size and remarkably higher AE and DL of the nanosystems, compared to the conventional fabrication. Microfluidics-produced NPs demonstrated to meet the safety requirements necessary to be intravenously administered, with special emphasis on the effectiveness of the nanoparticulate systems to avoid cytotoxicity in relation to the free form of EFV. Further functional targeting of NPs allowed to promote their deposition at the BBB, being expected to control the biodistribution of this anti-HIV drug. Although the functionalization strategy could not potentiate EFV permeability though the BBB, considerable improvements on the bioavailability of the drug at this biological site were achieved through the nanosystems, hopefully opening doors to future advances in therapies against HIV neuropathology. This work further lay the foundation for testing the efficacy of the nanofomulation developed on HIV-infected cell culture models, as well as under *in vivo* conditions, moving a step closer towards a translational DDS.

Acknowledgements

This article is a result of the project NORTE-01-0145-FEDER-000012, supported by Norte Portugal Regional Operational Programme (NORTE 2020), under the PORTUGAL 2020 Partnership Agreement, through the European Regional Development Fund (ERDF).

This work was financed by FEDER – Fundo Europeu de Desenvolvimento Regional funds through the COMPETE 2020 – Operacional Programme for Competitiveness and Internationalisation (POCI), Portugal 2020, Portuguese funds through FCT – Fundação para

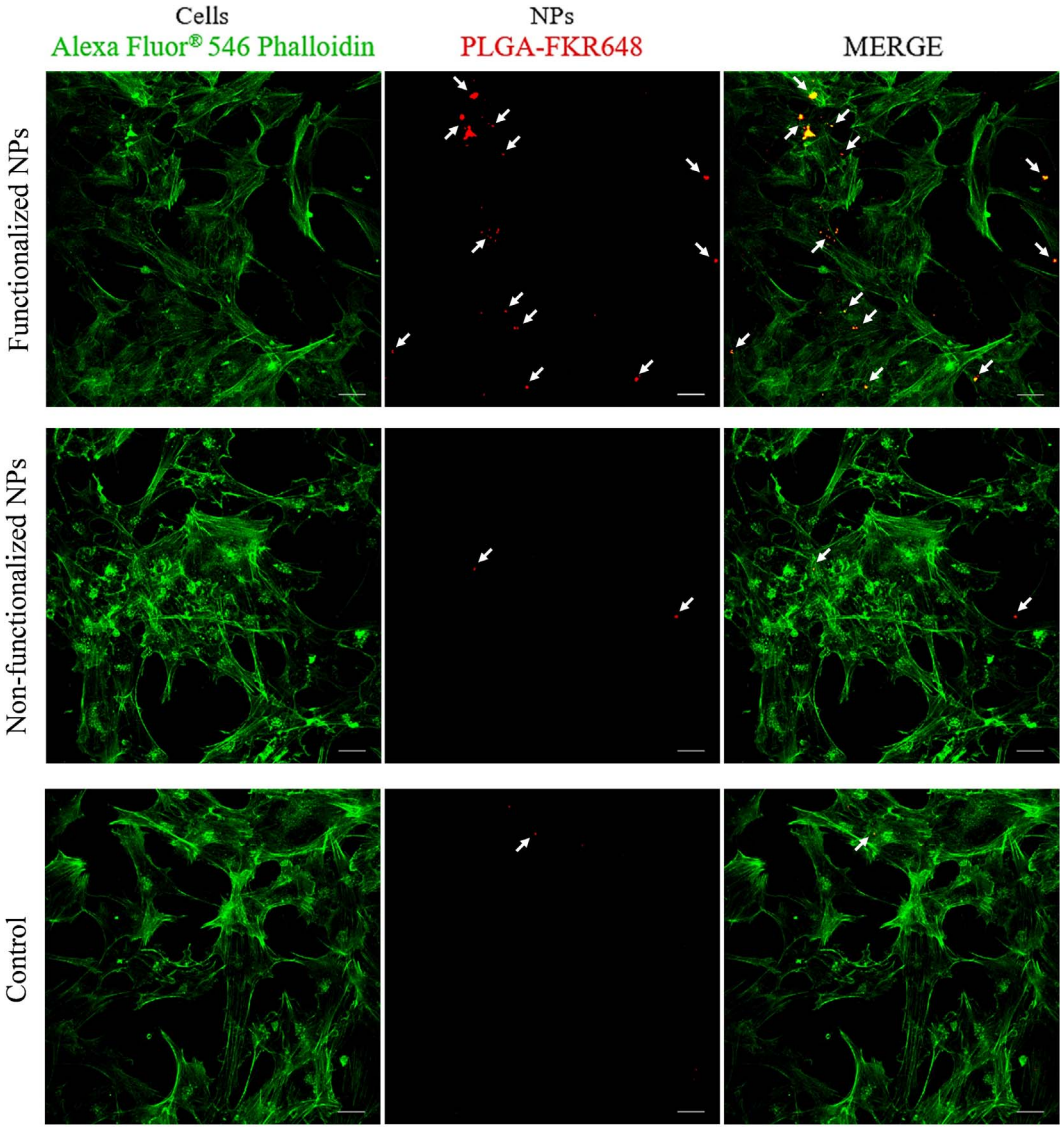

Fig. 10. The level of interaction between *h*CMEC/D3 cells and functionalized microfluidics-produced PLGA NPs was qualitatively analyzed through confocal microscopy (after 3 h of incubation). Cells are labeled in green, NPs in red. White arrows evidence NPs associated with cells. The control group consisted on the addition of free peptide prior to functionalized NPs (competition assay). Scale bars represent 20 μm.

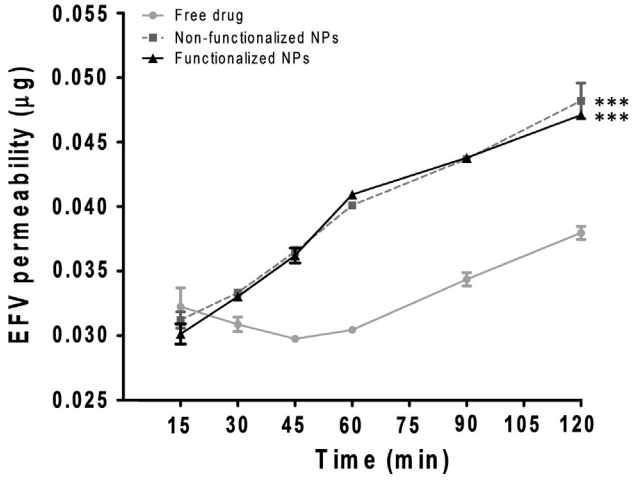

Fig. 11. Permeability of EFV in the free form, as well as loaded on non- or functionalized NPs, though a BBB *in vitro* model. Data were represented as mean ± SD ($n = 3$). *** denotes a significant difference ($p < .001$) when comparing the permeability of free EFV with EFV-loaded on both nanosystems.

a Ciência e a Tecnologia/Ministério da Ciência, Tecnologia e Ensino Superior in the framework of the project "Institute for Research and Innovation in Health Sciences" (POCI-01-0145-FEDER-007274), and by Interreg V-A Espanha-Portugal POCTEP Programme through FEDER funds from the European Union (0245_IBEROS_1_E).

The authors acknowledge the support of the Biointerfaces and Nanotechnology, Translational Cytometry, Biochemical and Biophysical Technologies, Histology and Electron Microscopy, and Bioimaging i3S Scientific Platforms.

Francisca Araújo, Maria João Gomes, Carlos Fernandes and Rute Nunes would like to thank to FCT for financial support (SFRH/BD/87016/2012, SFRH/BD/90404/2012, SFRH/BD/98519/2013 and SFRH/BD/96519/2013, respectively).

The authors would also like to express their gratefulness to José das Neves (i3S, Portugal), Patrick Kennedy (i3S, Portugal), Marco Araújo (i3S, Portugal), Virgínia Gonçalves (CESPU, Portugal) and Inês Castro Gonçalves (i3S, Portugal) for insightful feedback on the design of experiments.

Declarations of interest

None.

Appendix A. Supplementary material

Supplementary data associated with this article can be found, in the online version, at https://doi.org/10.1016/j.ejpb.2018.01.014.

References

[1] V. Valcour, P. Sithinamsuwan, S. Letendre, B. Ances, Pathogenesis of HIV in the central nervous system, Curr. HIV/AIDS Rep. 8 (2011) 54–61.
[2] N.J. Abbott, L. Ronnback, E. Hansson, Astrocyte-endothelial interactions at the blood-brain barrier, Nat. Rev. Neurosci. 7 (2006) 41–53.
[3] S.A. Pathan, Z. Iqbal, S.M. Zaidi, S. Talegaonkar, D. Vohra, G.K. Jain, A. Azeem, N. Jain, J.R. Lalani, R.K. Khar, F.J. Ahmad, CNS drug delivery systems: novel approaches, Recent Pat. Drug. Deliv. Formul. 3 (2009) 71–89.
[4] E. Vazquez, Sustiva (efavirenz) is approved, Posit Aware 9 (1998) 17.
[5] S. Sierra, B. Kupfer, R. Kaiser, Basics of the virology of HIV-1 and its replication, J. Clin. Virol. 34 (2005) 233–244.
[6] S.G. Sarafianos, B. Marchand, K. Das, D.M. Himmel, M.A. Parniak, S.H. Hughes, E. Arnold, Structure and function of HIV-1 reverse transcriptase: molecular mechanisms of polymerization and inhibition, J. Mol. Biol. 385 (2009) 693–713.
[7] D.D. Richman, HIV chemotherapy, Nature 410 (2001) 995–1001.
[8] M.J. Gomes, J. Neves, B. Sarmento, Nanoparticle-based drug delivery to improve the efficacy of antiretroviral therapy in the central nervous system, Int. J. Nanomed. 9 (2014) 1757–1769.
[9] I.U. Khan, C.A. Serra, N. Anton, T. Vandamme, Microfluidics: a focus on improved cancer targeted drug delivery systems, J. Control. Release 172 (2013) 1065–1074.
[10] C. Saraiva, C. Praça, R. Ferreira, T. Santos, L. Ferreira, L. Bernardino, Nanoparticle-mediated brain drug delivery: overcoming blood-brain barrier to treat neurodegenerative diseases, J. Control. Release 235 (2016) 34–47.
[11] M. Nair, R.D. Jayant, A. Kaushik, V. Sagar, Getting into the brain: potential of nanotechnology in the management of NeuroAIDS, Adv. Drug Deliv. Rev. 103 (2016) 202–217.
[12] A. Kaushik, R.D. Jayant, R. Nikkhah-Moshaie, V. Bhardwaj, U. Roy, Z. Huang, A. Ruiz, A. Yndart, V. Atluri, N. El-Hage, K. Khalili, M. Nair, Magnetically guided central nervous system delivery and toxicity evaluation of magneto-electric nanocarriers, Sci. Rep. 6 (2016) 25309.
[13] R.D. Jayant, V.S.R. Atluri, S. Tiwari, S. Pilakka-Kanthikeel, A. Kaushik, A. Yndart, M. Nair, Novel nanoformulation to mitigate co-effects of drugs of abuse and HIV-1 infection: towards the treatment of NeuroAIDS, J. Neurovirol. 23 (2017) 603–614.
[14] F. Danhier, E. Ansorena, J.M. Silva, R. Coco, A. Le Breton, V. Préat, PLGA-based nanoparticles: an overview of biomedical applications, J. Control. Release 161 (2012) 505–522.
[15] C. Martins, F. Sousa, F. Araújo, B. Sarmento, Functionalizing PLGA and PLGA derivatives for drug delivery and tissue regeneration applications, Adv. Healthc. Mater. (2017), http://dx.doi.org/10.1002/adhm.201701035.
[16] M.M. Yallapu, B.K. Gupta, M. Jaggi, S.C. Chauhan, Fabrication of curcumin encapsulated PLGA nanoparticles for improved therapeutic effects in metastatic cancer cells, J. Colloid Interface Sci. 351 (2010) 19–29.
[17] J.-M. Lim, R. Karnik, Optimizing the discovery and clinical translation of nanoparticles: could microfluidics hold the key? Nanomedicine 9 (2014) 1113–1116.
[18] L. Luo, T. Qin, Y. Huang, S. Zheng, R. Bo, Z. Liu, J. Xing, Y. Hu, J. Liu, D. Wang, Exploring the immunopotentiation of Chinese yam polysaccharide poly (lactic-co-glycolic acid) nanoparticles in an ovalbumin vaccine formulation in vivo, Drug. Deliv. 24 (2017) 1099–1111.
[19] G.M. Whitesides, The origins and the future of microfluidics, Nature 442 (2006) 368–373.
[20] S. Garg, G. Heuck, S. Ip, E. Ramsay, Microfluidics: a transformational tool for nanomedicine development and production, J. Drug Target. 24 (2016) 821–835.
[21] Q. Feng, J. Sun, X. Jiang, Microfluidics-mediated assembly of functional nanoparticles for cancer-related pharmaceutical applications, Nanoscale 8 (2016) 12430–12443.
[22] M.V. Bandulasena, G.T. Vladisavljević, O.G. Odunmbaku, B. Benyahia, Continuous synthesis of PVP stabilized biocompatible gold nanoparticles with a controlled size using a 3D glass capillary microfluidic device, Chem. Eng. Sci. 171 (2017) 233–243.
[23] F. Araujo, N. Shrestha, M.-A. Shahbazi, D. Liu, B. Herranz-Blanco, E.M. Mäkilä, J.J. Salonen, J.T. Hirvonen, P.L. Granja, B. Sarmento, Microfluidic assembly of a multifunctional tailorable composite system designed for site specific combined oral delivery of peptide drugs, ACS Nano 9 (2015) 8291–8302.
[24] D. Liu, H. Zhang, B. Herranz-Blanco, E. Mäkilä, V.P. Lehto, J. Salonen, J. Hirvonen, H.A. Santos, Microfluidic assembly of monodisperse multistage pH-responsive polymer/porous silicon composites for precisely controlled multi-drug delivery, Small 10 (2014) 2029–2038.
[25] L.Y. Chu, J.W. Kim, R.K. Shah, D.A. Weitz, Monodisperse thermoresponsive microgels with tunable volume-phase transition kinetics, Adv. Funct. Mater. 17 (2007) 3499–3504.
[26] J. das Neves, B. Sarmento, Precise engineering of dapivirine-loaded nanoparticles for the development of anti-HIV vaginal microbicides, Acta Biomater. 18 (2015) 77–87.
[27] C. Cunha-Reis, A. Machado, L. Barreiros, F. Araujo, R. Nunes, V. Seabra, D. Ferreira, M.A. Segundo, B. Sarmento, J. Das Neves, Nanoparticles-in-film for the combined vaginal delivery of anti-HIV microbicide drugs, J. Control. Release 243 (2016) 43–53.
[28] M.J. Gomes, P.J. Kennedy, S. Martins, B. Sarmento, Delivery of siRNA silencing P-gp in peptide-functionalized nanoparticles causes efflux modulation at the blood–brain barrier, Nanomedicine 12 (2017) 1385–1399.
[29] M.J. Gomes, C. Fernandes, S. Martins, F. Borges, B. Sarmento, Tailoring lipid and polymeric nanoparticles as siRNA carriers towards the blood-brain barrier–from targeting to safe administration, J. Neuroimmune Pharmacol. 12 (2016) 107–119.
[30] A.M. Pinto, C. Gonçalves, D.M. Sousa, A.R. Ferreira, J.A. Moreira, I.C. Gonçalves, F.D. Magalhães, Smaller particle size and higher oxidation improves biocompatibility of graphene-based materials, Carbon 99 (2016) 318–329.
[31] M.-A. Shahbazi, M. Hamidi, E.M. Mäkilä, H. Zhang, P.V. Almeida, M. Kaasalainen, J.J. Salonen, J.T. Hirvonen, H.A. Santos, The mechanisms of surface chemistry effects of mesoporous silicon nanoparticles on immunotoxicity and biocompatibility, Biomaterials 34 (2013) 7776–7789.
[32] B. Mendes, C. Marques, I. Carvalho, P. Costa, S. Martins, D. Ferreira, B. Sarmento, Influence of glioma cells on a new co-culture in vitro blood–brain barrier model for characterization and validation of permeability, Int. J. Pharm. 490 (2015) 94–101.
[33] A.S. Utada, A. Fernandez-Nieves, H.A. Stone, D.A. Weitz, Dripping to jetting transitions in coflowing liquid streams, Phys. Rev. Lett. 99 (2007) 094502.
[34] H. Xie, J.W. Smith, Fabrication of PLGA nanoparticles with a fluidic nanoprecipitation system, J. Nanobiotechnol. 8 (2010) 18.
[35] D.B. Weibel, G.M. Whitesides, Applications of microfluidics in chemical biology, Curr. Opin. Chem. Biol. 10 (2006) 584–591.
[36] X. Tian, F. Wei, T. Wang, P. Wang, X. Lin, J. Wang, D. Wang, L. Ren, In vitro and in vivo studies on gelatin-siloxane nanoparticles conjugated with SynB peptide to increase drug delivery to the brain, Int. J. Nanomed. 7 (2012) 1031–1041.
[37] R. Alyautdin, I. Khalin, M.I. Nafeeza, M.H. Haron, D. Kuznetsov, Nanoscale drug delivery systems and the blood–brain barrier, Int. J. Nanomed. 9 (2014) 795–811.
[38] K. Gao, X. Jiang, Influence of particle size on transport of methotrexate across blood brain barrier by polysorbate 80-coated polybutylcyanoacrylate nanoparticles, Int. J. Pharm. 310 (2006) 213–219.
[39] R. Karnik, F. Gu, P. Basto, C. Cannizzaro, L. Dean, W. Kyei-Manu, R. Langer, O.C. Farokhzad, Microfluidic platform for controlled synthesis of polymeric nanoparticles, Nano Lett. 8 (2008) 2906–2912.
[40] E. Dashtimoghadam, H. Mirzadeh, F.A. Taromi, B. Nyström, Microfluidic self-assembly of polymeric nanoparticles with tunable compactness for controlled drug delivery, Polymer 54 (2013) 4972–4979.
[41] A. Valério, D.S. Conti, P.H. Araújo, C. Sayer, S.R. da Rocha, Synthesis of PEG-PCL-based polyurethane nanoparticles by miniemulsion polymerization, Colloids Surf. B 135 (2015) 35–41.
[42] S. Stolnik, M. Garnett, M. Davies, L. Illum, M. Bousta, M. Vert, S. Davis, The colloidal properties of surfactant-free biodegradable nanospheres from poly(β-malic acid-co-benzyl malate)s and poly(lactic acid-co-glycolide), Colloids Surf. A 97 (1995) 235–245.
[43] D. Liu, S. Cito, Y. Zhang, C.F. Wang, T.M. Sikanen, H.A. Santos, A versatile and robust microfluidic platform toward high throughput synthesis of homogeneous nanoparticles with tunable properties, Adv. Mater. 27 (2015) 2298–2304.
[44] L. Martín-Banderas, E. Sáez-Fernández, M.Á. Holgado, M.M. Durán-Lobato, J.C. Prados, C. Melguizo, J.L. Arias, Biocompatible gemcitabine-based nanomedicine engineered by Flow Focusing for efficient antitumor activity, Int. J. Pharm. 443 (2013) 103–109.
[45] J. Della Rocca, D. Liu, W. Lin, Are high drug loading nanoparticles the next step forward for chemotherapy? Nanomedicine 7 (2012) 303–305.
[46] D. Liu, H. Zhang, S. Cito, J. Fan, E.M. Mäkilä, J.J. Salonen, J. Hirvonen, T.M. Sikanen, D.A. Weitz, H.A. Santos, Core/shell nanocomposites produced by superfast sequential microfluidic nanoprecipitation, Nano Lett. 17 (2017) 606–614.
[47] K. Chandra Hembram, S. Prabha, R. Chandra, B. Ahmed, S. Nimesh, Advances in preparation and characterization of chitosan nanoparticles for therapeutics, Artif. Cells Nanomed. Biotechnol. 44 (2016) 305–314.
[48] K. Grodowska, A. Parczewski, Analytical methods for residual solvents determination in pharmaceutical products, Acta Pol. Pharm. 67 (2010) 13–26.
[49] P. Sansdrap, A. Moes, In vitro evaluation of the hydrolytic degradation of dispersed and aggregated poly(DL-lactide-co-glycolide) microspheres, J. Control. Release 43 (1997) 47–58.
[50] F. Araújo, N. Shrestha, M.-A. Shahbazi, P. Fonte, E.M. Mäkilä, J.J. Salonen, J.T. Hirvonen, P.L. Granja, H.A. Santos, B. Sarmento, The impact of nanoparticles on the mucosal translocation and transport of GLP-1 across the intestinal epithelium, Biomaterials 35 (2014) 9199–9207.
[51] J. Emami, H. Hamishehkar, A.R. Najafabadi, K. Gilani, M. Minaiyan, H. Mahdavi, A. Nokhodchi, A novel approach to prepare insulin-loaded poly(lactic-co-glycolic acid) microcapsules and the protein stability study, J. Pharm. Sci. 98 (2009) 1712–1731.
[52] S. Salatin, J. Barar, M. Barzegar-Jalali, K. Adibkia, F. Kiafar, M. Jelvehgari, Development of a nanoprecipitation method for the entrapment of a very water soluble drug into Eudragit RL nanoparticles, Res Pharm Sci 12 (2017) 1–14.
[53] J. das Neves, M. Amiji, M.F. Bahia, B. Sarmento, Assessing the physical–chemical properties and stability of dapivirine-loaded polymeric nanoparticles, Int. J. Pharm. 456 (2013) 307–314.
[54] I. Takeuchi, K. Tomoda, A. Hamano, K. Makino, Effects of physicochemical properties of poly(lactide-co-glycolide) on drug release behavior of hydrophobic drug-loaded nanoparticles, Colloids Surf. A 520 (2017) 771–778.
[55] A. Trapani, J. Sitterberg, U. Bakowsky, T. Kissel, The potential of glycol chitosan nanoparticles as carrier for low water soluble drugs, Int. J. Pharm. 375 (2009)

97–106.
[56] S. Gao, J. Li, C. Jiang, B. Hong, B. Hao, Plasmid pORF-hTRAIL targeting to glioma using transferrin-modified polyamidoamine dendrimer, Drug. Des. Devel. Ther. 10 (2016) 1–11.
[57] F. Araújo, C. Martins, C. Azevedo, B. Sarmento, Chemical modification of drug molecules as strategy to reduce interactions with mucus, Adv. Drug. Deliv. Rev. (2017), http://dx.doi.org/10.1016/j.addr.2017.1009.1020.
[58] G. Platzer, M. Okon, L.P. McIntosh, pH-dependent random coil (1)H, (13)C, and (15)N chemical shifts of the ionizable amino acids: a guide for protein pK a measurements, J. Biomol. NMR 60 (2014) 109–129.
[59] V. Sanna, I.A. Siddiqui, M. Sechi, H. Mukhtar, Resveratrol-loaded nanoparticles based on poly(epsilon-caprolactone) and poly(d, l-lactic-co-glycolic acid)–poly (ethylene glycol) blend for prostate cancer treatment, Mol. Pharm. 10 (2013) 3871–3881.
[60] K. Gellynck, V. Kodeck, E. Van De Walle, K. Kersemans, F. De Vos, H. Declercq, P. Dubruel, L. Vlaminck, M. Cornelissen, First step toward near-infrared continuous glucose monitoring: in vivo evaluation of antibody coupled biomaterials, Exp. Biol. Med. 240 (2015) 446–457.
[61] E.H. Decloedt, G. Maartens, Neuronal toxicity of efavirenz: a systematic review, Expert. Opin. Drug. Saf. 12 (2013) 841–846.
[62] K. Amin, R.M. Dannenfelser, In vitro hemolysis: guidance for the pharmaceutical scientist, J. Pharm. Sci. 95 (2006) 1173–1176.
[63] S.A. McClave, Nutritional assessment in inflammatory bowel disease: application of nutrition strategies to the management of the difficult Crohn's patient, Am. J. Gastroenterol. 102 (2007) S88–S93.
[64] E.M. Damm, L. Pelkmans, J. Kartenbeck, A. Mezzacasa, T. Kurzchalia, A. Helenius, Clathrin- and caveolin-1-independent endocytosis: entry of simian virus 40 into cells devoid of caveolae, J. Cell Biol. 168 (2005) 477–488.
[65] F. Fekri, R.C. Delos Santos, R. Karshafian, C.N. Antonescu, Ultrasound microbubble treatment enhances clathrin-mediated endocytosis and fluid-phase uptake through distinct mechanisms, PLoS One 11 (2016) e0156754.
[66] T. Kang, M. Jiang, D. Jiang, X. Feng, J. Yao, Q. Song, H. Chen, X. Gao, J. Chen, Enhancing glioblastoma-specific penetration by functionalization of nanoparticles with an iron-mimic peptide targeting transferrin/transferrin receptor complex, Mol. Pharm. 12 (2015) 2947–2961.
[67] B. Weksler, E. Subileau, N. Perriere, P. Charneau, K. Holloway, M. Leveque, H. Tricoire-Leignel, A. Nicotra, S. Bourdoulous, P. Turowski, Blood-brain barrier-specific properties of a human adult brain endothelial cell line, FASEB J. 19 (2005) 1872–1874.
[68] C. Förster, M. Burek, I.A. Romero, B. Weksler, P.O. Couraud, D. Drenckhahn, Differential effects of hydrocortisone and TNFα on tight junction proteins in an in vitro model of the human blood–brain barrier, J. Physiol. 586 (2008) 1937–1949.
[69] H. Qosa, H. LeVine, J.N. Keller, A. Kaddoumi, Mixed oligomers and monomeric Amyloid-β disrupts endothelial cells integrity and reduces monomeric amyloid-β transport across hCMEC/D3 cell line as an in vitro blood-brain barrier model, BBA 2014 (1842) 1806–1815.
[70] M.A. Kaisar, R.K. Sajja, S. Prasad, V.V. Abhyankar, T. Liles, L. Cucullo, New experimental models of the blood-brain barrier for CNS drug discovery, Expert Opin. Drug Discov. 12 (2017) 89–103.
[71] J.J. Jamieson, P.C. Searson, S. Gerecht, Engineering the human blood-brain barrier in vitro, J Biol Eng 11 (2017) 37.
[72] S.T. Buckley, S.M. Fischer, G. Fricker, M. Brandl, In vitro models to evaluate the permeability of poorly soluble drug entities: challenges and perspectives, Eur. J. Pharm. Sci. 45 (2012) 235–250.
[73] A. Patabendige, The value of in vitro models of the blood–brain barrier and their uses, Altern. Lab. Anim. 40 (2012) 335–338.
[74] I. Wilhelm, C. Fazakas, I.A. Krizbai, In vitro models of the blood-brain barrier, Acta Neurobiol. Exp. 71 (2011) 113–128.
[75] G. Xu, S. Mahajan, I. Roy, K.T. Yong, Theranostic quantum dots for crossing blood-brain barrier in vitro and providing therapy of HIV-associated encephalopathy, Front. Pharmacol. 4 (2013) 140.
[76] M. Gregori, M. Masserini, S. Mancini, Nanomedicine for the treatment of Alzheimer's disease, Nanomedicine 10 (2015) 1203–1218.
[77] G. Graverini, V. Piazzini, E. Landucci, D. Pantano, P. Nardiello, F. Casamenti, D.E. Pellegrini-Giampietro, A.R. Bilia, M.C. Bergonzi, Solid lipid nanoparticles for delivery of andrographolide across the blood-brain barrier: in vitro and in vivo evaluation, Colloids Surf. B 161 (2018) 302–313.
[78] T.E. McGraw, F.R. Maxfield, Human transferrin receptor internalization is partially dependent upon an aromatic amino acid on the cytoplasmic domain, Cell Regul. 1 (1990) 369–377.
[79] M.D. Chavanpatil, A. Khdair, J. Panyam, Nanoparticles for cellular drug delivery: mechanisms and factors influencing delivery, J. Nanosci. Nanotechnol. 6 (2006) 2651–2663.
[80] L.M. Bareford, P.W. Swaan, Endocytic mechanisms for targeted drug delivery, Adv. Drug Deliv. Rev. 59 (2007) 748–758.
[81] N.P. Gabrielson, D.W. Pack, Efficient polyethylenimine-mediated gene delivery proceeds via a caveolar pathway in HeLa cells, J. Control. Release 136 (2009) 54–61.